Electromagnetic Science
vol. x, no. x, , May xxxx
https://doi.org/10.23919/emsci.2023.0007

Communication

Wideband Microstrip Antenna in Small Volume without Using Fundamental Mode

Yongjian Zhang[1] and Yue Li[1,2]

1. *Department of Electronic Engineering, Tsinghua University, Beijing 100084, China*
2. *Beijing National Research Center for Information Science and Technology, Tsinghua University, Beijing 10084, China*

Corresponding author: Yue Li, Email: lyee@tsinghua.edu.cn.
Received March 2, 2023; Accepted May 5, 2023

Abstract — Microstrip antennas are of significant interest and extensively utilized in communication systems because of their unique low profile. However, the general difficulty in microstrip antenna design lies in its wideband electromagnetic radiation within a low-profile structure. To enhance the bandwidth, superposing the fundamental mode and other high-order modes is the most common method, but this occupies a larger footprint than regular narrow-band modes. Here, as a counterintuitive way to broaden the bandwidth, a wideband miniaturized microstrip antenna is proposed by using two high-order modes. The avoidance of the fundamental mode allows for footprint miniaturization without decreasing the bandwidth, providing a different but feasible design strategy for wideband microstrip antennas. Compared with other microstrip antennas at the same profile, the proposed antenna achieves wider bandwidth and a smaller footprint. The experimental result shows a bandwidth of 4.81–6.01 GHz is achieved with a volume of 0.47×0.47×0.043 λ_0^3, where λ_0 represents the in-vacuum wavelength at the center frequency. Therefore, the proposed design provides an effective solution to the intrinsic contradiction between wideband electromagnetic radiation and compact antenna dimensions, not only in a low profile but in a small footprint, contributing to the fundamental development of microstrip antennas.

Keywords — Microstrip antennas, Wideband antennas, High-order modes, Low profile, Small footprint.
Citation — Yongjian Zhang and Yue Li, "Wideband Microstrip Antenna in Small Volume without Using Fundamental Mode," *Electromagnetic Science*, vol. x, no. x, article no. , xxxx. doi: 10.23919/emsci.2023.0007.

I. Introduction

Microstrip antennas have received extensive academic research and attention recently owing to their appealing benefits, including low profile, easy integration, low cost and ability to develop high-gain and multipolarized antennas [1]. Nevertheless, a regular microstrip antenna is limited by its narrow bandwidth. Here, we define an antenna bandwidth where the reflection coefficient at the antenna input port is lower than -10 dB. Therefore, such a narrow bandwidth has difficulty meeting the evolving requirements of wireless communication and navigation systems. It has been theoretically proven that the compact volume (including the profile and footprint) and wide bandwidth of an antenna are inherently contradictory [2]. Techniques have been developed to enhance the microstrip antenna bandwidth by using parasitic structures [3]–[7]. A resonant slot can be utilized in a microstrip antenna, realizing a bandwidth higher than 40% [3]. By etching the patch into an E-shape, a microstrip antenna can obtain a bandwidth of 30.3% [4]. In addition, the antenna design in Ref. [5] adopted an L-shaped feeding structure and achieved a bandwidth wider than 35%. As another regular method, a stacked patch structure can also enhance the bandwidth of a microstrip antenna [6], [7].

In recent decades, the technique of merging multiple operating modes with different frequencies has been widely investigated to broaden the operating bandwidth of microstrip antennas. For a microstrip antenna positioned in the *XoY* plane and perpendicular to the *Z*-axis, a series of TM_{mn} modes with different numbers of *m* and *n* can be excited for electromagnetic wave radiation. Here, the TM_{mn} mode refers to the mode where the electric field shows a distribution of *m* half wavelengths along the *X*-axis and *n* half wavelengths along the *Y*-axis. Among the various TM_{mn} modes, the TM_{10} mode is the fundamental mode with the lowest operating frequency and a relatively wider bandwidth [8]–[10]. Hence, as the most common candidate for multimode cooperation, the TM_{10} mode is indispensable for superposition with other high-order modes. Many examples have successfully enhanced the bandwidth by adopting this fundamental mode [11]–[23]. A slot-loaded microstrip antenna in Ref.[11] excited its TM_{10} and TM_{01} modes, providing a bandwidth of 3.8% within a profile of 0.01 λ_0, where λ_0 represents the wavelength in vacuum at the center

frequency. Several wideband microstrip antennas with grid-slotted patches incorporate the TM_{10} and anti-TM_{20} modes in Refs.[12]–[15]. Furthermore, a slot–strip structure with a Y-shaped feeding line or matching branches [16]–[18] was proposed to broaden bandwidths larger than 40%. In Ref.[19], a slot–patch structure with shorting vias is presented and excited at the TM_{10} and TM_{12} modes. It realized a bandwidth of 10% within a 0.039 λ_0 profile. A slot-loaded microstrip antenna with a profile of 0.048 λ_0 in Ref.[20] also utilized TM_{10} and TM_{12} modes, reaching an operating bandwidth of 14%. A millimeter-wave microstrip antenna that superposed the TM_{30} and TM_{10} modes broadened the bandwidth to 18% in a low profile of 0.05 λ_0 [21]. Three operating modes, including the TM_{10}, anti-TM_{20} and TM_{30} modes, were simultaneously incorporated in Ref.[22] over a broad bandwidth of 75% within a volume of 0.8×0.72×0.24 λ_0^3. These multimode low-profile microstrip antennas provided a wide operating bandwidth by occupying a footprint area larger than 0.5×0.5 λ_0^2, which may be limited for space-limited systems or array arrangements with low grating lobes. Therefore, there is still a general challenge in microstrip antenna design due to the wide operating bandwidth and compact antenna volume, including not only a low profile but also a small footprint area.

In this paper, we propose a wideband microstrip antenna with a small footprint and low profile. Compared with existing microstrip antennas, the proposed antenna achieves a wide bandwidth by using two high-order modes without using the fundamental mode. Specifically, this design excites an anti-TM_{20} mode and an anti-TM_{02} mode, which are superposed to realize a wide bandwidth with properly placed blind vias. The final antenna design has a small footprint of 0.47×0.47 λ_0^2 and a low profile of 0.043 λ_0. The measured results show that the proposed antenna realizes gain stabilization in a wide bandwidth of 22.2%. Moreover, the antenna also provides a front-to-back ratio (the difference between the gains of forward radiation along the $+Z$-axis and backward radiation along the $-Z$-axis) higher than 16 dB. In short, the proposed microstrip antenna design provides an efficacious solution to simultaneously implement wide bandwidth and compact volume, providing a feasible solution for antenna research in space-limited situations.

II. Operating Principle

The geometric configuration of the proposed microstrip antenna is illustrated in Figure 1, with the optimized dimensions listed in Table 1. As shown in Figure 1(a), the presented antenna consists of a slot-gridded patch, a metal ground, an L-shaped feeding probe, and eight metallic blind vias. As the radiating aperture, the patch is printed on a 0.813-mm-thick Rogers RO4003C dielectric substrate named Layer 1 with a relative permittivity of 3.55. As shown in Figures 1(b) and 1(c), the patch is divided into four subpatches with a side length of w by two perpendicular etched slots with a width of g. The L-shaped probe is composed of an upper patch printed on a 1.524-mm-thick Rogers RO4003C dielectric substrate named Layer 2 and an offset metallic cylinder column through Layer 2. Eight metallic blind vias are properly and symmetrically located through Layer 2 and connected to the metallic ground with dimensions of 60×60 mm^2. As depicted in Figure 1(d), the total antenna profile is h_1+h_2=2.34 mm, which is 0.043 λ_0 at the center frequency of 5.4 GHz.

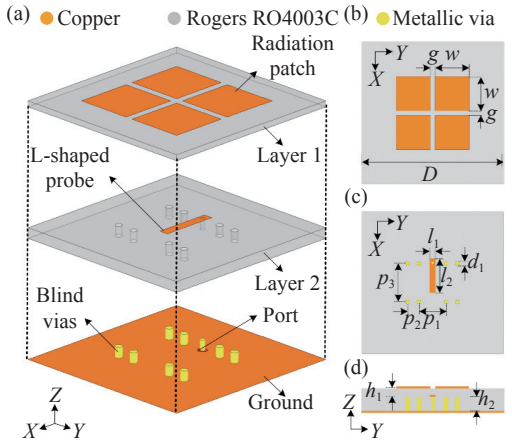

Figure 1 Geometry configuration of the proposed microstrip antenna. (a) Exploded view of the antenna. (b) Top view of Layer 1. (c) Top view of Layer 2. (d) Side view of the antenna.

Table 1 Detailed dimensions (Unit: mm)

w	g	l_1	l_2	d_1	D
12	1.6	2	12	1.5	60
p_1	p_2	p_3	h_1	h_2	
9.6	4	13.6	0.813	1.624	

Compared with other conventional wideband microstrip antennas using the fundamental TM_{10} mode, the adopted anti-TM_{20} mode and anti-TM_{02} mode in the proposed design are depicted in Figure 2. In the anti-TM_{20} mode shown in Figure 2(a), the electric field is anti-phase double-half-wavelength distributed along the X-axis. An obvious reversal of the electric field occurs at the position of the slot. The electric field is uniformly distributed along the Y-axis. A pair of parallel magnetic currents denoted by the purple dotted double arrows in Figure 2(a) is equivalently generated on the radiating aperture, providing a broadside copolarized radiation pattern. Figure 2(b) shows the anti-TM_{02} mode at a higher frequency. Different from the regular TM_{02} mode, the electric field in the anti-TM_{02} mode shows an anti-phase zero-order mode along the X-axis but regular second-order mode along the Y-axis. The electric field on the radiating aperture serves as a pair of parallel magnetic currents denoted by the purple dotted double arrows in Figure 2(b), also generating a broadside pattern with copolarization. In addition, four magnetic currents are equivalently generated by the anti-phase uniform electric field on the other two sides of the radiation patch

structure, which are denoted by the green dotted double arrows in Figure 2(b). These magnetic currents are symmetrical but reversed, cancelling the radiation field and generating a gain null along the *Z*-direction in the far field. Hence, a cross-polarized conical radiation pattern exists in the anti-TM_{02} mode. The initial formulas of the resonant frequency of the anti-TM_{20} mode and anti-TM_{02} mode can be expressed as

$$f_{\text{anti-TM}_{20}} = \frac{c}{2\pi}\sqrt{k_{x_1}^2 + k_{y_1}^2 + k_{z_1}^2} \tag{1}$$

$$f_{\text{anti-TM}_{02}} = \frac{c}{2\pi}\sqrt{k_{x_2}^2 + k_{y_2}^2 + k_{z_2}^2} \tag{2}$$

where k_{y1} and k_{z1} are equal to zero due to the uniform electric field distribution of the anti-TM_{20} mode along the *X*- and *Z*-axes, and k_{z2} is also equal to zero in the anti-TM_{02} mode. However, k_{x2} is nonzero because the cross-slot structure disturbs the uniform field of the anti-TM_{02} mode along the *X*-axis and provides an inverse of the electric field, which can be equivalently regarded as a parasitic capacitor. Hence, the resonant frequency of the anti-TM_{02} mode is larger than that of the anti-TM_{20} mode, leading to dual-band operation.

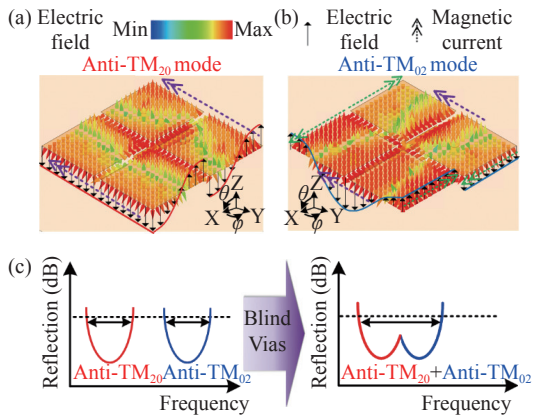

Figure 2 Operating modes of the proposed microstrip antenna. Electric field distribution of the (a) anti-TM_{20} mode and (b) anti-TM_{02} mode in the simulation diagrams. (c) Operating bands before and after involvement of metallic blind vias.

To merge these modes together for a wide bandwidth, eight metallic blind vias are utilized, with the results depicted in Figure 2(c). These eight blind vias are arranged at the center point of each subpatch along the *X*-axis, i.e., the null of the electric field in the anti-TM_{20} mode, and located symmetrically off-center point of each subpatch along the *Y*-axis. Hence, the blind vias are equivalently regarded as several capacitors in the anti-TM_{02} mode but have little effect on the anti-TM_{20} mode. To illustrate the operating mechanism more clearly, the equivalent circuit of the antenna in the anti-TM_{02} mode is illustrated in Figure 3(a). According to the classic model of the microstrip antenna, the radiating apertures can be modeled as parallel R-L-C circuits. C_e and L_e represent the equivalent capacitance and inductor of the field along the patch edge, and R denotes the radiating resistor. The symmetrical structure results in symmetry in the equivalent circuit model. The blind vias can be regarded as parallel capacitors, which are denoted by C_b. Due to the off-center point configuration of the blind vias along the *Y*-axis, the parallel capacitors C_b are loaded at the nonzero point of the electric field in the anti-TM_{02} mode. The value of parallel capacitors C_b can be obtained by the calculation formula of plate capacitance. Hence, the capacitance is proportional to the area between the radiation patch and the upper surface of the blind vias, i.e., a larger radius of blind vias leads to a larger parallel capacitance. Owing to the involvement of these blind vias, the electric field under the radiation patch and the current distribution on the patch are greatly affected, leading to the resonant frequency of the anti-TM_{02} mode moving lower. Thus, by adjusting the position and size of the blind vias, the separated operating bands of the anti-TM_{20} mode and anti-TM_{02} mode can be superposed to be a broadened frequency band compared with any single mode. It is worth mentioning that no extra footprint or profile is occupied in the proposed wideband

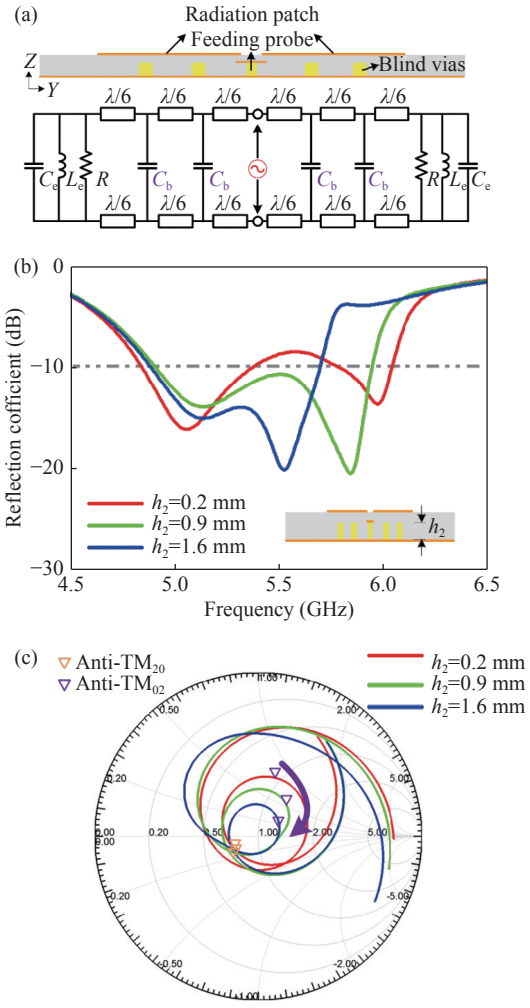

Figure 3 (a) Equivalent circuit of the antenna in the anti-TM_{02} mode. Influence of blind vias on the operating band. (b) Reflection coefficient. (c) Input port impedance on the Smith chart.

microstrip antenna design. Moreover, the size of the metal ground has a negligible impact on the radiation performance, indicating that the proposed antenna maintains stable operating modes with metal grounds of varying sizes. On basis of this design strategy, the proposed antenna can be further investigated to be ultralow-profile or more compact. Such a small antenna volume is feasible for arrays with low grating lobes and space-limited systems.

Then, the critical parameters of the metallic blind vias are studied to further verify the operating mechanism of the proposed method. Here, the influence of the via height on the operating frequency band is mainly studied and analyzed. Figure 3 illustrates the simulated reflection coefficients and input port impedance of the presented antenna with different via heights h_2. The Smith chart in Figure 3(c) is a common and useful diagram that can directly reflect the changes in antenna input port impedance [23]. As seen, a larger value of the height h_2 indicates a narrower distance between the blind vias and radiation patch, thus leading to a larger parallel capacitance (shown as the purple arrow in Figure 3(c)) in the anti-TM_{02} mode. Hence, a lower resonant frequency of the anti-TM_{02} mode is obtained in Figure 3(b). By regulating the value of height h_2 from 0.2 mm to 1.6 mm, the resonant frequency of the anti-TM_{02} mode decreases from 6.0 GHz to 5.5 GHz accordingly. However, the resonant frequency of the anti-TM_{20} mode remains stable (shown as the orange triangle in Figure 3(c)), indicating that the blind vias have little impact on the anti-TM_{20} mode. Therefore, we can adjust the resonant frequency of the anti-TM_{02} mode by optimizing the blind vias to regulate the operating bandwidth of the proposed antenna until the widest operating bandwidth is achieved.

III. Experimental Results

A prototype is built and measured to verify the proposed design method. As depicted in Figure 4(a), a 50-Ω semi-grid cable is adopted to feed the presented antenna, with the inner conductor soldered to the metallic cylinder column of the L-shaped probe and outer conductor soldered to the metallic ground. Without loss of generality, the square ground area is selected as 60×60 mm^2, with little impact on the electromagnetic performances of the proposed antenna. The whole antenna is fabricated on a Rogers RO4003C substrate with a relative permittivity of 3.55 by the printed circuit board (PCB) process. Eight 1-mm-radius plastic cylinder columns with a relative permittivity of 3.0 are utilized to tightly clamp the two dielectric substrate layers. The presented microstrip antenna is numerically simulated and optimized in the commercial electromagnetic simulation software HFSS 2018.0. The fabricated prototype is tested by using an N9917A vector network analyzer and a standard microwave anechoic chamber. In practical systems, a shunt inductor with a large value of inductance can be loaded at the feeding port to provide electrostatic discharge (ESD).

The reflection coefficients of the presented microstrip antenna in the measured and simulated results are depicted

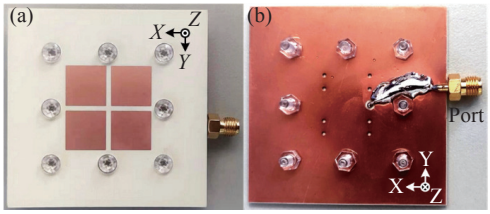

Figure 4 Photographs of the fabricated microstrip antenna. (a) Top view. (b) Back view.

in Figure 5. Owing to the superposition of the anti-TM_{20} and anti-TM_{02} modes, the measured −10-dB impedance bandwidth spans from 4.81 GHz to 6.01 GHz, i.e., a fractional bandwidth of 22.2%. A slight deterioration of the operating frequency band between the simulated and experimental results mainly contributes to the air gap between the two dielectric substrate layers, which can be avoided by using multilayer-board processing technology.

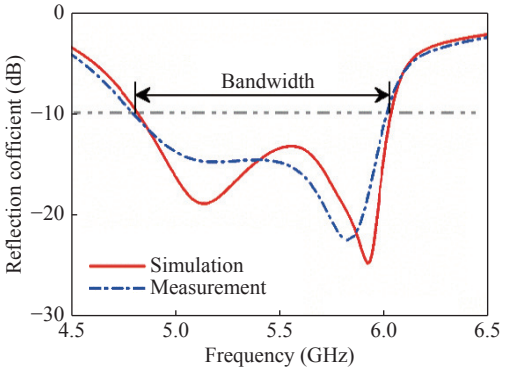

Figure 5 Reflection coefficients of the proposed microstrip antenna in simulated and measured results.

Figure 6 illustrates the radiation performances of the presented antenna. The radiation patterns in the *YoZ* and *XoZ* planes at the resonant frequency point of the anti-TM_{20} mode, i.e., 5.14 GHz, are shown in Figures 6(a) and 6(b). A broadside copolarized radiation pattern is realized with a front-to-back ratio larger than 21 dB. Figures 6(c) and 6(d) show the radiation patterns at 5.92 GHz, which is the resonant frequency of the anti-TM_{02} mode. Broadside radiation is also achieved with a front-to-back ratio larger than 16 dB. Here, a cross-polarized conical radiation pattern exists in the *YoZ* plane in the anti-TM_{02} mode due to the symmetrical but reverse magnetic current mentioned above. The realized gain and total efficiency are also measured and shown in Figure 7. The simulated peak realized gain ranges from 5.06 dBi to 7.98 dBi, and the total efficiency is higher than 84% in the whole band. In the measured result, the fabricated antenna achieves a realized gain varying from 5.0 dBi to 7.6 dBi in the band, indicating that the antenna provides wideband gain stabilization. In addition, the measured efficiency is higher than 82% in the band, which is consistent with the simulated efficiency.

To highlight the contribution of the presented microstrip antenna, Table 2 presents a comparison in terms of

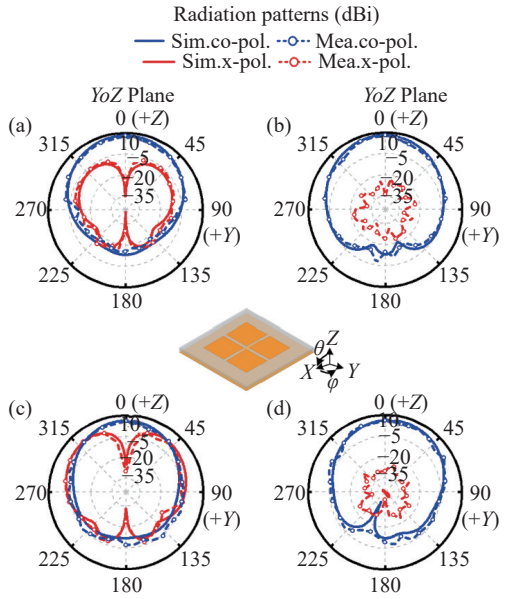

Figure 6 Radiation patterns in simulation and measurement. Radiation patterns in the (a) *YoZ* and (b) *XoZ* planes at 5.14 GHz. Radiation patterns in the (c) *YoZ* and (d) *XoZ* planes at 5.92 GHz.

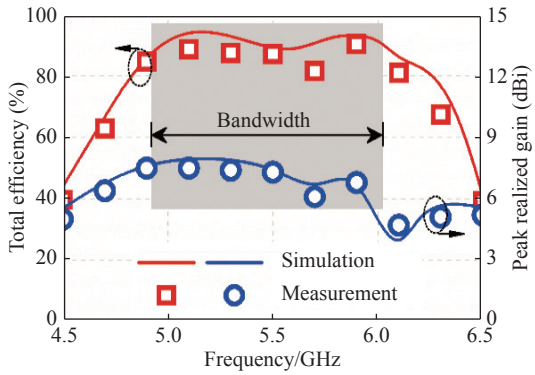

Figure 7 Total efficiencies and peak realized gains of the proposed antenna in simulated and measured results.

footprint area, antenna profile, and operating bandwidth with other wideband microstrip antennas with similar profiles. All microstrip antenna designs in Refs.[14], [15], and [18]–[21] superpose the TM_{10} mode and other high-order modes to broaden the antenna bandwidth. TM_{10} and anti-TM_{20} modes are incorporated within the grid-slotted patch structure in Ref.[14], realizing a bandwidth of 25%. The microstrip antenna in Ref.[15] adopts the same operating mode to achieve a bandwidth of 21.3% in a lower profile of 0.045 λ_0. The TM_{12} mode is utilized with the fundamental mode for multimode cooperation in Refs.[19], [20], providing a bandwidth higher than 10%. A higher-order mode named the TM_{30} mode is used in Ref.[21] to obtain a bandwidth of 18% in a profile of 0.052 λ_0. Different from the antenna designs in these studies, the proposed wideband microstrip antenna only adopts two high-order operating modes instead of the fundamental TM_{10} mode. It can be observed that the antenna designs in Refs.[14], [15], [19] occupy a larger footprint area to achieve broad bandwidth, whereas the proposed wideband microstrip antenna only occupies a footprint smaller than 0.5×0.5 λ_0^2, which is suitable for space-limited applications and array formation without grating lobes. In addition, the proposed microstrip antenna also provides a wider bandwidth than Refs.[20], [21] in a similar volume. To our knowledge, the proposed antenna realizes the smallest footprint area with a similar bandwidth and profile. This fact indicates that although the fundamental mode has a wider bandwidth than other single high-order modes, it occupies the entire footprint with half the operating wavelength. However, superposing other high-order modes together achieves even wider bandwidth in a smaller volume. In short, the proposed microstrip antenna without using the fundamental mode provides a feasible solution to simultaneously realize wide bandwidth and compact volume, advancing the fundamental development of microstrip antennas.

Table 2 Comparison among the proposed antenna design and other wideband microstrip antennas with similar profiles.

Ref.	Footprint area (λ_0^2)	Profile (λ_0)	Bandwidth
[14]	1.1×1.1	0.06	25%
[15]	0.75×0.75	0.045	21.3%
[18]	0.88×0.78	0.11	24.8%
[19]	1.17×0.5	0.039	10%
[20]	0.58×0.39	0.048	14%
[21]	0.59×0.41	0.052	18%
Proposed	**0.47×0.47**	**0.043**	**22.2%**

IV. Conclusion

In this work, a wideband but compact microstrip antenna is proposed by using two high-order modes, i.e., the anti-TM_{20} mode and anti-TM_{02} mode. Eight metal blind vias are arranged under the slot-gridded patch to merge these two modes for wideband operation. The measured result shows an impedance bandwidth of 4.81–6.01 GHz with broadside radiation within a miniaturized volume of 0.47×0.47×0.043 λ_0^3. Compared with other microstrip antennas at the same profile, the proposed antenna achieves wider bandwidth but with a smaller footprint. Hence, the proposed design strategy, avoiding the fundamental mode, provides a feasible method for footprint miniaturization but bandwidth enhancement in wideband microstrip antennas, contributing to the fundamental advancement of the microstrip antenna field.

Acknowledgment

This work was supported by the National Natural Science Foundation of China (U22B2016 and 62022045), the National Key Research and Development Program of China (2021 YFA0716600), and the Shenzhen Science and Technology Program (JSGG20210802153800002).

References

[1] D. M. Pozar, "Microstrip antennas," *Proceedings of the IEEE*, vol. 80, no. 1, pp. 79–91, 1992.

[2] W. Geyi, "Physical limitations of antenna," *IEEE Transactions on Antennas and Propagation*, vol. 51, no. 8, pp. 2116–2123, 2003.

[3] T. Huynh and K. F. Lee, "Single-layer single-patch wideband microstrip antenna," *Electronics Letters*, vol. 31, no. 16, pp. 1310–1312, 1995.

[4] F. Yang, X. X. Zhang, X. N. Ye, *et al*., "Wide-band E-shaped patch antennas for wireless communications," *IEEE Transactions on Antennas and Propagation*, vol. 49, no. 7, pp. 1094–1100, 2001.

[5] K. M. Luk, C. L. Mak, Y. L. Chow, *et al*., "Broadband microstrip patch antenna," *Electronics Letters*, vol. 34, no. 15, pp. 1442–1443, 1998.

[6] A. A. Serra, P. Nepa, G. Manara, *et al*., "A wide-band dual-polarized stacked patch antenna," *IEEE Antennas and Wireless Propagation Letters*, vol. 6, pp. 141–143, 2007.

[7] D. Sun, W. B. Dou, L. Z. You, *et al*., "A broadband proximity-coupled stacked microstrip antenna with cavity-backed configuration," *IEEE Antennas and Wireless Propagation Letters*, vol. 10, pp. 1055–1058, 2011.

[8] X. K. Liu, W. Hu, S. Gao, *et al*., "A wideband triple-mode differentially fed microstrip patch antenna," *IEEE Antennas and Wireless Propagation Letters*, vol. 20, no. 7, pp. 1160–1164, 2021.

[9] S. Yan, Y. Zheng, B. Y. Wang, *et al*., "A low-profile wideband microstrip antenna with pattern diversity based on composite right/left-handed transmission lines," *IEEE Antennas and Wireless Propagation Letters*, vol. 20, no. 8, pp. 1478–1482, 2021.

[10] S. Radavaram and M. Pour, "Wideband radiation reconfigurable microstrip patch antenna loaded with two inverted U-slots," *IEEE Transactions on Antennas and Propagation*, vol. 67, no. 3, pp. 1501–1508, 2019.

[11] S. Q. Xiao, B. Z. Wang, W. Shao, *et al*., "Bandwidth-enhancing ultralow-profile compact patch antenna," *IEEE Transactions on Antennas and Propagation*, vol. 53, no. 11, pp. 3443–3447, 2005.

[12] Y. M. Pan, P. F. Hu, X. Y. Zhang, *et al*., "A low-profile high-gain and wideband filtering antenna with metasurface," *IEEE Transactions on Antennas and Propagation*, vol. 64, no. 5, pp. 2010–2016, 2016.

[13] W. Y. Sun, Y. Li, L. Chang, *et al*., "Dual-Band dual-polarized microstrip antenna array using double-layer gridded patches for 5G millimeter-wave applications," *IEEE Transactions on Antennas and Propagation*, vol. 69, no. 10, pp. 6489–6499, 2021.

[14] W. Liu, Z. N. Chen, and X. Qing, "Metamaterial-based low-profile broadband mushroom antenna," *IEEE Transactions on Antennas and Propagation.*, vol. 62, no. 3, pp. 1165–1172, 2014.

[15] W. E. I. Liu, Z. N. Chen, and X. M. Qing, "Broadband low-profile L-probe fed metasurface antenna with TM leaky wave and TE surface wave resonances," *IEEE Transactions on Antennas and Propagation*, vol. 68, no. 3, pp. 1348–1355, 2020.

[16] W. Y. Sun, Y. Li, Z. J. Zhang, *et al*., "Broadband and low-profile microstrip antenna using strip-slot hybrid structure," *IEEE Antennas and Wireless Propagation Letters*, vol. 16, pp. 3118–3121, 2017.

[17] W. Y. Sun, Y. Li, Z. J. Zhang, *et al*., "Low-profile and wideband microstrip antenna using quasi-periodic aperture and slot-to-CPW transition," *IEEE Transactions on Antennas and Propagation*, vol. 67, no. 1, pp. 632–637,Jan, 2019.

[18] W. Y. Sun and Y. Li, "Gain stabilization method for wideband slot-coupled microstrip antenna," *IEEE Transactions on Antennas and Propagation*, vol. 69, no. 12, pp. 8932–8936, 2021.

[19] N. W. Liu, L. Zhu, W. W. Choi, *et al*., "A low-profile differential-fed patch antenna with bandwidth enhancement and sidelobe reduction under operation of TM_{10} and TM_{12} modes," *IEEE Transactions on Antennas and Propagation*, vol. 66, no. 9, pp. 4854–4859, 2018.

[20] C. L. Chen, "A wideband coplanar L-probe-fed slot-loaded rectangular filtering microstrip patch antenna with high selectivity," *IEEE Antennas and Wireless Propagation Letters*, vol. 21, no. 6, pp. 1134–1138, 2022.

[21] D. Wang, K. B. Ng, C. H. Chan, *et al*., "A novel wideband differentially-fed higher-order mode millimeter-wave patch antenna," *IEEE Transactions on Antennas and Propagation*, vol. 63, no. 2, pp. 466–473, 2015.

[22] J. W. Lian, D. Z. Ding, and R. S. Chen, "Wideband millimeter-wave substrate-integrated waveguide-fed metasurface antenna," *IEEE Transactions on Antennas and Propagation*, vol. 70, no. 7, pp. 5335–5344, 2022.

[23] Z. J. Zhang, *Antenna Design for Mobile Devices*, 2nd ed. , Wiley, Hoboken, NJ, USA, 2017.

Yongjian Zhang received a B.S. degree in Communication Engineering from Tongji University, Shanghai, China, in 2018. He is currently pursuing a Ph.D. degree in Electronic Engineering from Tsinghua University, Beijing, China. His current research interests include aircraft antennas, dual-polarized antennas, and multiple-input/multiple-output (MIMO) antenna arrays. He serves as a reviewer for the *IEEE Transactions on Antennas and Propagation*, *IEEE Antennas and Wireless Propagation Letters*, and *Microwave and Optical Technology Letters*.
(Email: zhangyj18@mails.tsinghua.edu.cn)

Yue Li received a B.S. degree in Telecommunication Engineering from the Zhejiang University, Zhejiang, China, in 2007, and a Ph.D. degree in Electronic Engineering from Tsinghua University, Beijing, China, in 2012. He is currently an Associate Professor in the Department of Electronic Engineering at Tsinghua University.

In June 2012, Dr. Li was a postdoctoral fellow in the Department of Electronic Engineering, Tsinghua University. In December 2013, he was a research scholar in the Department of Electrical and Systems Engineering, University of Pennsylvania. He was also a visiting scholar in Institute for Infocomm Research (IR), A*STAR, Singapore, in 2010, and the Hawaii Center of Advanced Communication (HCAC), University of Hawaii at Manoa, Honolulu, HI, USA, in 2012. Since January 2016, he has been with Tsinghua University, where he is an Assistant Professor. He has authored and coauthored over 200 journal papers and 50 international conference papers and holds 26 granted Chinese patents. His current research interests include metamaterials, plasmonics, electromagnetics, nanocircuits, mobile and handset antennas, MIMO and diversity antennas, and millimeter-wave antennas and arrays.

Dr. Li was a recipient of the Isaac Koga Gold Medal from the URSI General Assembly in 2017; the Second Prize of Science and Technology Award of China Institute of Communications in 2017; the Young Scientist Award from the conferences of Progress in Electromagnetics Research Symposium (PIERS) 2019, International Applied Computational Electromagnetics Society Symposium (ACES) 2018, Atlantic Radio Science Conference (AT-RASC) 2018, Asia-Pacific Radio Science Conference (AP-RASC) 2016, International Symposium on Electromagnetic Theory (EMTS) 2016, and URSI General Assembly and Scientific Symposium (GASS) 2014; the Best Paper Award from the conferences of PhotonIcs & Electromagnetics Research Symposium (PIERS) 2021, International Workshop on Electro-

magnetics (iWEM) 2021, Asia-Pacific Conference on Antennas and Propagation (APCAP) 2020 and 2017, UK-Europe-China Workshop on Millimeter Waves and Terahertz Technologies (UCMMT) 2020, International Symposium on Antennas and Propagation (ISAP) 2019, Cross Strait Quad-Regional Radio Science and Wireless Technology Conference (CSQRWC) 2018, International Symposium on Antennas, Propagation and EM Theory (ISAPE) 2021 and 2016, International Conference on Microwave and Millimeter Wave Technology (ICMMT) 2020 and 2016, National Conference on Microwave and Millimeter Waves (NCMMW) 2018 and 2017, National Conference on Antennas (NCANT) 2019 and 2017; the Outstanding Doctoral Dissertation of Beijing Municipality in 2013; and the Principal Scholarship of Tsinghua University in 2011. He is serving as an Associate Editor for the *IEEE Transactions on Antennas and Propagation*, *IEEE Antennas and Wireless Propagation Letters*, *Microwave and Optical Technology Letters*, and *Computer Applications in Engineering Education*. He is also serving on the Editorial Board of *Scientific Reports*, *Sensors*, and *Electronics*. (Email: lyee@tsinghua.edu.cn)